Circulating Current Suppression in Modular Multilevel Converters with Even-Harmonic Repetitive Control

Shunfeng Yang, *Student Member, IEEE,* Peng Wang, *Senior Member, IEEE,* Yi Tang, *Member*, *IEEE*, Michael Zagrodnik, Xiaolei Hu, *Member*, *IEEE*, and King Jet Tseng

***Abstract*—Due to the voltage mismatch between the phase legs and the DC bus in Modular Multilevel Converters (MMCs), the differential current in MMCs is inherently subjected to circulating even order harmonics. Repetitive control based active harmonic suppression methods can be adopted to eliminate such harmonics. Nevertheless, conventional repetitive controllers have a relatively slow dynamic response because all the sampled errors in the past one cycle have to be stored, which causes a response delay for one fundamental period. This paper proposes an improved repetitive control scheme that exclusively copes with even order harmonics based on the circulating current characteristics of MMC systems. The design details of the even harmonic repetitive control scheme according to the harmonics characteristics are provided. The proposed even-harmonic repetitive control scheme requires halved data memory to store error samplings and the delay introduced by the repetitive controller is also reduced. According to the frequency domain analysis, the even-harmonic repetitive control features faster convergence rate, greater low-frequency gains, higher crossover frequency, and higher tolerance against system frequency deviation, while possessing the same even-order harmonics suppression capability and stability as conventional ones. Simulation and experimental results are presented to show the steady-state harmonics suppression capability, dynamic response, and disturbance tolerance of the proposed even-harmonic repetitive control scheme.**

***Index Terms*—Modular Multilevel Converter, circulating current, even-harmonic repetitive control.**

I. Introduction

MODULAR Multilevel Converter (MMC) is one of the most attractive topologies in recent years for medium or high voltage industrial applications [1], such as high-voltage DC (HVDC) transmission [2, 3], medium voltage variable speed motor drives [4] and static synchronous compensators [5]. The wide adoption of MMCs in the industry is mainly due to its flexible expandability, transformer-less configuration, common DC bus, high reliability from redundancy, and so on. A well-known problem within an MMC system is that the differential current in phase legs may be distorted by even-order harmonics [6-8], and this is because of the inherent mismatch between the inserted voltage of each phase leg and the DC bus voltage. Such low order harmonics not only increase the current stress of semiconductors and introduce more power losses in phase legs, but also, in turn, bring disturbances on the sub-module capacitor voltage, which consequently deteriorate the performance of the MMC system [7, 9-11].

In most applications, the harmonics in the differential current of an MMC are undesirable from efficiency and controllability points of view, except for some special applications such as capacitor voltage ripple shaping [12, 13] and motor drives in low-frequency operations [14, 15]. Nevertheless, it is difficult to find a practical passive filter to mitigate these low-order harmonics in the differential current. Alternatively, some active harmonic suppression methods were proposed in recent literature such as compensating the inserted voltage in each phase leg based on open-loop control strategies [16, 17], injecting adequate harmonics by feedforward control to reduce the second order harmonics in the differential current [9]. However, these methods highly rely on accurate MMC models and are sensitive to the disturbance and model parameter variation. A simple proportional-integral (PI) controller based feedback control of the DC loop current is presented in [11], where obvious low-frequency AC components can still be found in the differential current. Feedback controls in the d-q or rotating frames were proposed in [8, 18, 19] for second order harmonic suppression of MMC systems. Alternatively, proportional-resonant (PR) controllers can also be adopted to deal with harmonics under both symmetric and unbalanced load conditions as discussed in [20, 21]. However, one evident limitation of those methods is that they can only cope with specific order harmonics, depending on the controller design. Recently, plug-in repetitive controllers, which have been widely used in PWM inverters [22, 23], are employed in [24-26] to eliminate multiple harmonics in the differential current of MMC systems. In [24] and [25], the conventional repetitive controllers with one fundamental period delay are employed to handle both odd and even order harmonics. Based on the integrating function of the repetitive controller, a differential current control system combining a repetitive controller with a

Manuscript received April 3, 2017; revised July 06, 2017; accepted August 26, 2017. This work was conducted with support from the National Research Foundation (NRF) Singapore under the Corp Lab@University Scheme. (Corresponding author: Yi Tang)

S. Yang, P. Wang, Y. Tang and K. J. Tseng are with the School of Electrical and Electronic Engineering, Nanyang Technological University, 50 Nanyang Avenue, 639798 Singapore (e-mail: syang012@e.ntu.edu.sg; epwang@ntu.edu.sg; yitang@ntu.edu.sg; k.j.tseng@pmail.ntu.edu.sg).

X. Hu is with the Rolls-Royce@NTU Corporate Lab, Nanyang Technological University, 50 Nanyang Avenue, 639798 Singapore (e-mail: XLHU@ ntu.edu.sg).

M. Zagrodnik is with Rolls-Royce Singapore Pte. Ltd., Singapore 797575 (e-mail: MichaelAdam.Zagrodnik@ Rolls-Royce.com).

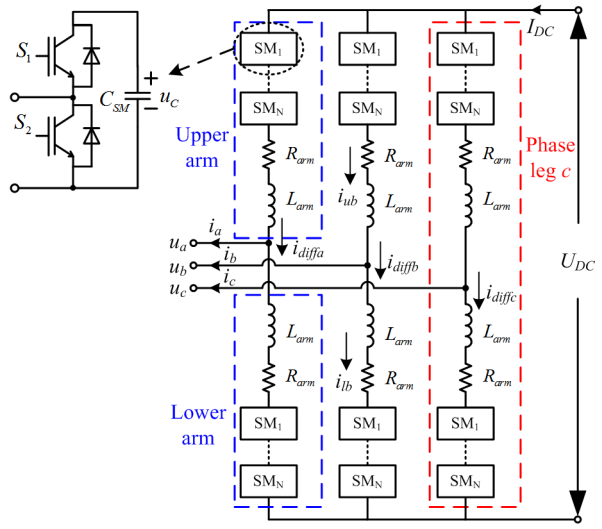

Fig. 1. Structure of a three-phase MMC based inverter.

proportional controller is proposed in [27], in order to facilitate the control system design and improve the accuracy and robustness of the control system.

In this paper, an improved repetitive controller being able to exclusively cope with the even-order signals is proposed for the sake of perfect even harmonics suppression in the differential current, based on the circulating current characteristics of the MMC system. The proposed repetitive controller has the same performance and system stability as conventional ones in terms of even-harmonic elimination. By halving the number of samplings stored in one repetitive cycle, it possesses additional benefits such as less memory occupation, a faster convergence rate, and a greater tolerance to system frequency variation as evidenced by the comprehensive frequency characteristics analysis in this paper. Full design details of the even harmonics repetitive control scheme, including selecting the number of error samples stored in each repetitive cycle to deal with the harmonics with specific frequencies, determining the crossover frequencies of the low pass filters in the repetitive controller according to the harmonic contents, and investigating the controller convergence rate and system stability, are provided. The effectiveness and validity of the proposed even-harmonic repetitive control scheme are confirmed in simulations and experiments. The results show that the proposed repetitive controller provides better circulating harmonics suppression than the PI and PR controllers. On the other hand, in comparison to the conventional repetitive controller, the dynamics of the proposed repetitive controller is almost doubled in the startup process and during reference or load step changes. Moreover, the even-harmonic repetitive controller also offers better harmonic suppression when there is a 5% system frequency deviation, compared with that of the conventional ones.

II. MMC Modelling and Differential Current Analysis

The basic structure and operation of an MMC have been extensively explained in the literature [11, 28] and will not be discussed in this paper. The schematic diagram of a three-phase MMC is shown in Fig. 1. There are three phase legs connected in parallel to a common DC bus and each phase leg consists of two arms, named as the upper arm and lower arm respectively. N sub-modules (SMs) are connected in series in the upper and lower arms respectively. Each arm is equipped with an arm inductor L_{arm} to prevent the parallel connection of two voltage sources, i.e. the DC-bus and the arm voltages. An equivalent resistor R_{arm} is employed in each arm to represent the losses on the semiconductors, equivalent series resistance (ESR) in C_{SM} and L_{arm}, etc. The output terminals of the MMC are the middle points of the two arms in the three phase legs.

According to the average model of the MMC and the analysis in [7, 11], the voltages and currents in the upper and lower arms in phase x ($x = a, b, c$) can be calculated as

$$\begin{cases} u_{ux} = NU_C\left[\dfrac{1-m_x\sin(\omega_o t+\phi_x)}{2}\right]-u_{diffx} \\ u_{lx} = NU_C\left[\dfrac{1+m_x\sin(\omega_o t+\phi_x)}{2}\right]-u_{diffx} \end{cases} \tag{1}$$

$$\begin{cases} i_{ux} = i_{diffx}+\dfrac{i_{ox}}{2} \\ i_{lx} = i_{diffx}-\dfrac{i_{ox}}{2} \end{cases} \tag{2}$$

where U_C is the average voltage across the sub-module capacitor, m_x=2U_{ox}/U_{DC} is the modulation index, ω_o denotes the fundamental angular frequency, ϕ_x stands for the phase angle of the output voltage, i_{diffx} refers to the differential current in the phase leg [12] and i_{ox} represents the output current of the MMC. The outputs of the MMC are

$$\begin{cases} u_{ox} = U_{ox}\sin(\omega_o t+\phi_x) \\ i_{ox} = I_{ox}\sin(\omega_o t+\phi_x+\phi_{ox}) \end{cases} \tag{3}$$

where U_{ox} and I_{ox} are the magnitudes of the output voltage and current respectively, and ϕ_{ox} is the phase displacement between the output voltage and current. u_{diffx} in (1) is defined as

$$u_{diffx} = L_{arm}\frac{di_{diffx}}{dt}+R_{arm}i_{diffx} = \frac{U_{DC}}{2}-\frac{u_{ux}+u_{lx}}{2} \tag{4}$$

It is clear in (4) that the voltage mismatch between the DC bus voltage U_{DC} and the voltage in the phase leg u_{ux}+u_{lx} will be eventually applied onto the arm inductors and resistors, and consequently introduces the inner differential current in the phase leg. In practice, such voltage mismatch is ineluctable owing to the voltage ripples on each sub-module capacitor [7, 10] and the PWM pattern of the actual voltage in the two arms. It should be noted that the differential voltage in phase x (u_{diffx}) is independently determined by the voltage inserted into the x phase. So that the differential voltages in the three phases can be analyzed independently as in three single-phase legs. In steady state, i_{diffx} normally consists of two parts as

$$i_{diffx} = \frac{I_{DC}}{3}+i_{cirx} \tag{5}$$

i.e., a DC current I_{DC}/3, assuming the DC source current I_{DC} is evenly split into the three phases, that ensures the power balance between the DC input and AC output [4], and a circulating current i_{cirx} that is dominated by even order harmonics [7, 10]. The detailed harmonic contents in the circulating current can be derived based on the circulating current analysis given in [7].

III. Even-Harmonic Repetitive Controller for MMC Differential Current Regulation

In most cases, only the DC component $I_{DC}/3$ in the differential current is preferred to maintain the stable operation of the MMC and minimize the losses. Therefore, in addition to controlling the output power of the MMC, special efforts are also devoted to the inner differential current control to remove i_{cirx}. According to (4) and (5), i_{diffx} can be controlled by legitimately adjusting the voltages u_{ux} and u_{lx} [8]. The s-domain transfer function of the plant can be expressed as

$$G(s)=\frac{1}{L_{arm}s+R_{arm}} \tag{6}$$

The block diagram of generating the differential current reference is shown inside the block (a) in Fig. 2. The differential current reference i_{diffx}^* is comprised of three components, i.e. a DC reference $i_{diffx\_DC}^*=m_x I_{ox}\cos(\phi_{ox})/4$ for power balance, a current reference $i_{diffx\_va}^*$ for voltage averaging control [11] to maintain the sub-module capacitor voltages at the same level, and a fundamental frequency current reference $i_{diffx\_vd}^*$ for the differential voltage control [6] between the upper and lower arms. u_C^* is the reference of the sub-module capacitor voltage defined as U_{DC}/N. U_{Cu} and U_{Cl} are the average capacitor voltages in the upper and lower arms respectively. The block (c) in Fig. 2 shows the process of generating the reference signals for individual sub-module as

$$u_{uxk/lxk}^*=\frac{1}{2}(1\mp u_{ox}^*)-u_{diffx}^*+u_{buxk/blxk}^* \tag{7}$$

where u_{diffx}^* is the reference voltage that will be applied to the arm inductors to control the differential current. Moreover, individual capacitor voltage balancing control [11] shown in Fig. 3 is also applied to ensure that the voltages across sub-module capacitors are balanced. $u_{buxk/blxk}^*$ is the reference for individual capacitor voltage balancing control and K_b is the gain of the proportional controller.

The circulating current i_{cirx} cannot be completely removed if only a conventional PI controller is employed as in Fig. 2 (b), for the sake of a tradeoff between the harmonic suppression and system stability. In order to properly regulate the differential current, a repetitive controller is adopted in the current control scheme instead of the single PI controller, as shown in Fig. 4, where $PI(z)$ is the z-domain transfer functions of the PI controller. The inherent computation and PWM delays in a digital control system are modeled as one sampling period delay and a zero-order-hold (ZOH) block respectively [29, 30].

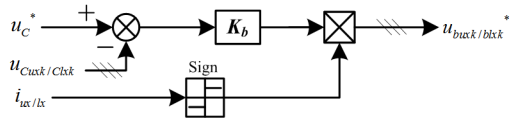

Fig. 3. Block diagram of individual capacitor voltage balancing control.

A. Proposed Even-Harmonic Repetitive Controller

Repetitive Controllers (RCs) are effective in dealing with periodic signals, e.g. tracking periodic reference or rejecting periodic disturbances. The structure of the repetitive controller adopted in this paper is highlighted in the dotted block in Fig. 4. The sampled error i_{diff_err} will be stored for N_s sampling intervals and then fed back to the plant again. By doing so, the gains of the repetitive controller at characteristic frequencies will be high enough to effectively control the signals at these frequencies, at the cost of relatively slow response and N_s memory cell occupation. With the presence of time delay block z^{-N_s}, the repetitive controller output generated based on the tracking error is postponed by a time period of N_sT_s seconds [31]. The transfer function of the repetitive controller can be expressed as

$$G_{rc}(z)=\frac{K_r z^k S(z)}{z^{N_s}-Q(z)} \tag{8}$$

where K_r is the repetitive gain, $Q(z)$ is a low-pass filter with unity gain at low frequencies and no phase delay. The low pass filter $Q(z)$ is employed to reject high-frequency components in the internal model [22, 31]. The phase lead filter, consisting of a low pass filter $S(z)$ and a phase delay compensation unit z^k [22, 23, 32], is used to improve the stability of the overall repetitive control system. However, high-frequency signals cannot be

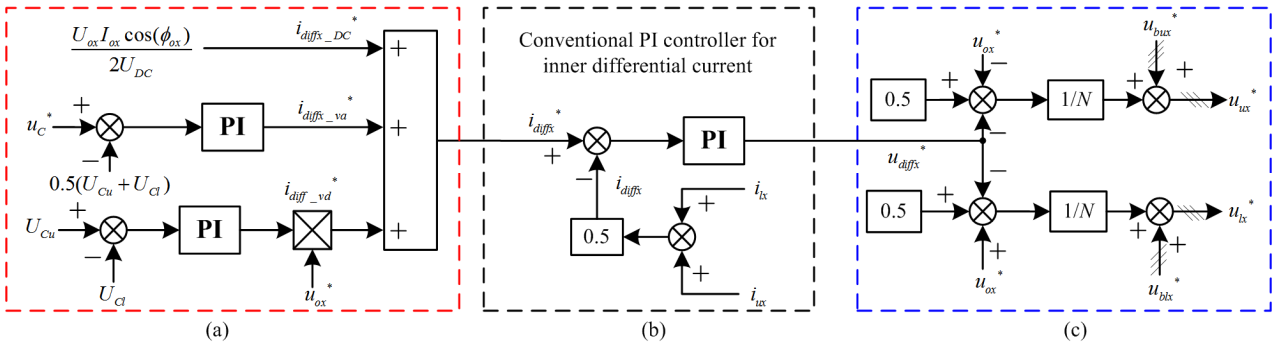

Fig. 2. Block diagram of the differential current control of the MMC and reference generation for each sub-module.

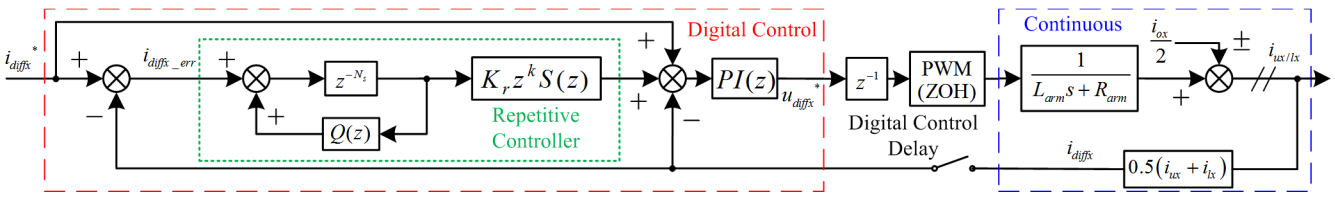

Fig. 4. Block diagram of the repetitive control scheme for inner differential current control of the MMC.

compensated due to the presence of $Q(z)$ and $S(z)$, which brings a trade-off between the tracking accuracy and the system robustness [22, 33].

Since there are only even order harmonics exist in the circulating current, it is rational that a repetitive controller exclusively coping with even harmonics, which is rarely addressed in the literature as the even harmonics exist in few application, is elaborately designed to suppress the circulating current ripples in the differential current. The frequency response of $G_{rc}(z)$ can be expressed as

$$G_{rc}(e^{j\omega T_s}) = \frac{K_r e^{jk\omega T_s} S(e^{j\omega T_s})}{e^{j\omega N_s T_s} - Q(e^{j\omega T_s})} \tag{9}$$

Since $Q(e^{j\omega T_s}) \approx 1$ at the frequencies lower than its cutoff frequency ω_c, the repetitive controller has high gains at frequencies as

$$\omega = \frac{2k\pi}{N_s T_s}, \quad 0 < k < \frac{\omega_c}{\omega_o} \tag{10}$$

where k is an integer. As the sampling interval of a control system is usually set to be constant, a repetitive controller can be designed to cope with different orders of harmonics by setting $N_s = 2l\pi/\omega_o T_s = lf_s/f_o$, where f_s is the sampling frequency and f_o is the output frequency. For a conventional repetitive controller designed to cope with odd and even harmonics, N_s is selected to be $N_s = f_s/f_o$. In this paper, the even order harmonic repetitive controller can be achieved by setting the number of error samples N_s to be half of that in one fundamental period, i.e. $N_s = f_s/(2f_o)$. Compared to the conventional repetitive controllers, the even-harmonic repetitive controller has high gains at frequencies that are the even multiples of f_o, while the memory cells required to store these samples are halved and the delay of the repetitive controller is reduced. The magnitude and phase characteristics of the conventional and proposed even-harmonic repetitive controllers are compared in Fig. 5, which shows that the proposed controller has high gains at even-order frequencies with less phase delay. Moreover, the performance of the repetitive controller is also improved compared with the conventional ones, which will be discussed in terms of frequency characteristics analysis in the next subsection.

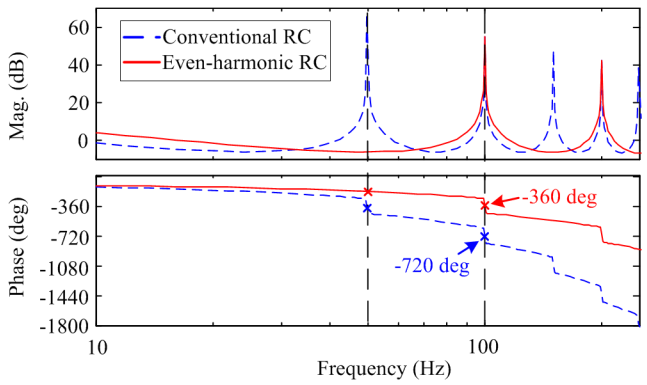

Fig. 5. Bode diagrams of the conventional and even-harmonic repetitive controllers.

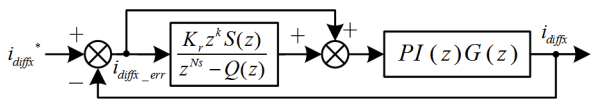

Fig. 6. Simplified block diagram of the differential current control loop.

B. *Analysis of the Even-Harmonic Repetitive Controller*

In order to analyze the differential current control scheme more conveniently and effectively, the overall differential current control loop is eventually simplified as in Fig. 6. The closed-loop transfer function from the reference to the differential current can be derived as

$$i_{diff} = \frac{P(z)\left[z^{N_s} - Q(z) + K_r z^k S(z)\right]}{z^{N_s} - Q(z) + K_r z^k S(z) P(z)} i_{diff}^* \tag{11}$$

where $P(z)$ is the closed loop transfer function of the PI control loop. The differential current tracking error can be derived according to (11), as

$$i_{err} = \frac{[1 - P(z)]\left[z^{N_s} - Q(z)\right]}{z^{N_s} - Q(z) + K_r z^k S(z) P(z)} i_{diff}^* \tag{12}$$

According to (11) and (12), the repetitive control system is stable if all the roots of the system characteristic equation z^{Ns}-$Q(z)$+$K_r z^k S(z)P(z)$ are located inside the unit circle at the origin. One sufficient condition [34] for the stability of the repetitive control system is

$$\left|Q(z) - K_r z^k S(z) P(z)\right| < 1 \tag{13}$$

The stability of this control system will not be influenced by choosing different values of N_s, as N_s does not appear in this inequality. As stated in [22], the current tracking error convergence can be derived from (12) as

$$z^{N_s} i_{err} \approx \left[Q(z) - K_r z^k S(z) P(z)\right] i_{err} \tag{14}$$

It is evident from (14) that the tracking error of the repetitive control scheme will be $|Q(z)$-$K_r z^k S(z)P(z)|i_{err}$ after a time period of $N_s T_s$. The convergence rate of the proposed repetitive controller is accordingly doubled because of the halved N_s compared with that of the conventional repetitive controllers.

As shown in Fig. 6, the overall control system can be simply divided into two parallel forward paths, i.e. a simple PI controller applied to the plant model, and a repetitive controller cascaded with the PI controller and the plant model. In this paper, only the path including the repetitive controller is analyzed and discussed. The transfer function of the repetitive controller path and the controller itself are described as

$$G_{RP}(z) = G_{rc}(z) PI(z) G(z) \tag{15}$$

It is clear in (8) and (15) that N_s will affect the open loop gain of the repetitive control path. Since the open loop gain of the repetitive control path is proportional to that of $G_{rc}(z)$, only $G_{rc}(z)$ is discussed here. As the high-frequency gain of a repetitive controller is normally designed to be small to prevent oscillation, only the low-frequency gain is investigated. The magnitude of the time advance unit z^k is one so that it will not affect the gain of the repetitive controller. The low pass filter $S(z)$ is also dedicatedly designed with almost unity gain at low frequencies. Therefore, the gain of $G_{rc}(z)$ can be rewritten as in (16) when $\omega << \omega_c$.

$$|G_{rc}(e^{j\omega T_s})| \approx \frac{K_r}{|e^{j\omega N_s T_s} - Q(e^{j\omega T_s})|} \tag{16}$$

Noting that when ω is low, $Q(e^{j\omega T_s})$ is very close to one, so that the open loop gain of this repetitive controller can be further simplified as

$$|G_{rc}(e^{j\omega T_s})| \approx \frac{K_r}{|e^{j\omega N_s T_s}-1|} = \frac{K_r}{|\cos(\omega N_s T_s)+j\sin(\omega N_s T_s)-1|} = \frac{K_r}{2}\frac{1}{|\sin(\omega N_s T_s/2)|} \tag{17}$$

Substituting $N_s = f_s/f_o$ and $N_s = f_s/2f_o$ into (17) respectively and noting that $T_s f_s = 1$, it can be found that the gain of the even-harmonic repetitive controller is almost twice of that of the conventional repetitive controller when $f << 2f_o$ as indicated in (18).

$$\frac{|G_{rc}(e^{j\omega T_s})|_{N_s=f_s/2f_o}}{|G_{rc}(e^{j\omega T_s})|_{N_s=f_s/f_o}} \approx \frac{|\sin(\pi f/f_o)|}{|\sin(\pi f/2f_o)|} \approx 2 \tag{18}$$

Equation (19) shows that the crossover frequency of the repetitive controller f_{cross} is inversely proportional to N_s.

$$f_{cross} = \left.\frac{\arcsin(K_r/2)}{\pi N_s T_s}\right|_{0\le K_r\le 2,\ \omega T_s \approx 0} \tag{19}$$

Furthermore, the phase-frequency characteristics of the repetitive controller can be derived based on (9) as

$$\angle G_{rc}(e^{j\omega T_s}) = k\omega T_s + \angle S(e^{j\omega T_s}) - \angle[e^{j\omega N_s T_s} - Q(e^{j\omega T_s})] \approx k\omega T_s + \angle S(e^{j\omega T_s}) - \angle(e^{j\omega N_s T_s}-1) \tag{20}$$

The critical frequencies for the proposed even-harmonic repetitive controller are those satisfying nf_o with n being an even integer. The magnitude of $G_{rc}(z)$ will cross 0 dB at these frequencies. The corresponding phase displacements of the proposed and conventional repetitive controllers as

$$\angle G_{rc}(e^{j\omega T_s})\big|_{N_s=f_s/2f_o} - \angle G_{rc}(e^{j\omega T_s})\big|_{N_s=f_s/f_o} \approx \angle(e^{j2\pi f/f_o}-1) - \angle(e^{j\pi f/f_o}-1) = n\pi \qquad n = 0, 2, 4\cdots \tag{21}$$

indicating that the proposed even-harmonic repetitive controller introduces less phase delay compared to that of the conventional one, as presented in Fig. 5. Meanwhile, it could be conveniently verified by (16) that the gains of $G_{rc}(z)$ at desired frequencies (e.g. 100 Hz, 200 Hz…) are also not affected no matter the value of N_s is selected to be f_s/f_o or $f_s/2f_o$. The bandwidth of the proposed repetitive controller f_B at critical even-order frequencies can also be derived by assigning -3 dB to the magnitude of $G_{rc}(z)$, as

$$f_B = \left.\frac{2\arcsin(K_r/1.416)}{\pi N_s T_s}\right|_{0\le K_r\le 2,\ \omega T_s \approx 0} \tag{22}$$

It is obvious that f_B is inversely proportional to N_s as well at low frequencies. Wider bandwidth is helpful in offering better tolerance for system frequency deviation. For instance, a frequency deviation f_d may be introduced making the MMC output frequency to be actually $f = f_o \pm f_d$, the magnitude of $G_{rc}(e^{j\omega T_s})$ at relatively low frequencies can be expressed by

$$|G_{rc}(e^{j\omega T_s})| \approx \frac{K_r}{2}\frac{1}{|\sin(n\pi(f_o \pm f_d)N_s T_s)|} \approx \frac{K_r}{2n\pi f_d N_s T_s} \tag{23}$$

where n is an even integer and $n\pi f_d << f_o$. Substituting $N_s = f_s/f_o$ and $N_s = f_s/2f_o$ into (23), the results indicate that the gains of the even-harmonic repetitive controller at deviated frequencies are twice of those of the conventional controller. In other words, the proposed repetitive controller has wider bandwidths at critical frequencies and consequently better compensating performance when there is a system frequency variation. The magnitude characteristics of both the conventional and the even-harmonic repetitive controllers are depicted in Fig. 7. It can be seen that the frequency characteristics of $G_{rc}(z)$, in terms of low-frequency gain, crossover frequency, magnitudes, and bandwidths at desired frequencies, etc., are in accordance with the mathematical analysis.

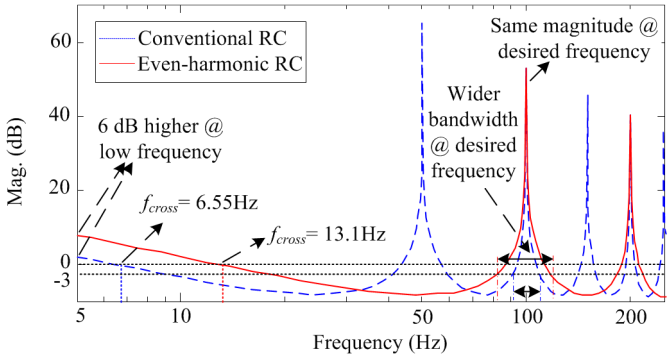

Fig. 7. The frequency characteristics of $G_{rc}(z)$ with $N_s = f_s/f_o$ and $N_s = f_s/2f_o$.

C. Even-harmonic Repetitive Control Scheme Design

The detailed parameters of the MMC system are listed in Table I. As the equivalent switching frequency of the MMC is $6f_c$ = 12 kHz [11], the sampling frequency is designed to be f_s = 12 kHz and the control system is synchronized with it, having a period of $T_s = 1/f_s$. N_s is chosen to be 120 to perform the even-harmonic repetitive controller. A phase-shifted PWM (PS-PWM) modulation scheme is employed to generate corresponding gating signals for individual sub-modules. In order to implement the individual control to every sub-module, an individual voltage reference and a phase-shifted triangular carrier are assigned to each sub-module. The phase displacement of triangular carriers for sub-modules in one arm is $2\pi/N$. By doing this, the output voltage level is $2N$+1 and the equivalent switching frequency is $2Nf_c$, where f_c is the carrier frequency and N is an odd number [11, 35].

The discrete transfer function of the plant can be converted from $G(s)$ by ZOH transform [29], as

$$G(z) = \frac{1}{R_{arm}}\left(\frac{1-e^{-T_s R_{arm}/L_{arm}}}{z-e^{-T_s R_{arm}/L_{arm}}}\right) \tag{24}$$

The closed conventional PI differential current control loop

TABLE I
PARAMETERS OF THE MMC SYSTEM

Parameters	Values
DC link voltage: U_{DC}	240 V
Amplitude of Output Voltage	100 V
Load Resistor: R_l	10 Ω
Load Inductor: L_l	6.3 mH
Rated output frequency: f_o	50 Hz
No. SM in each arm: N	3
Arm inductance: L_{arm}	5 mH
Arm resistor: R_{arm}	0.025 Ω
SM capacitor: C_{SM}	470 uF
Carrier frequency: f_c	20k Hz
PI parameters of the difference current control	K_p = 3, K_i = 10
Repetitive controller gain: K_r	0.8

can be treated as the plant of the repetitive controller, whose transfer function can be derived as

$$P(z)=\frac{PI(z)G(z)z^{-1}}{1+PI(z)G(z)z^{-1}} \tag{25}$$

According to the circulating current contents analysis presented in [7], the amplitude of the circulating current higher than 500 Hz (the 10^{th} order) is negligible in the MMC system employed in this paper, the cut-off frequencies of the low-pass filters in the repetitive controller can be designed appropriately. The low pass filter $Q(z)$ is designed as

$$Q(z)=\frac{z^2+z+4+z^{-1}+z^{-2}}{8} \tag{26}$$

The frequency response of $Q(z)$ can be written as

$$Q(e^{j\omega T_s})=\frac{2\cos^2(\omega T_s)+\cos(\omega T_s)+1}{4} \tag{27}$$

The cutoff frequency of $Q(z)$ is designed to be around 940 Hz, which is almost nineteen times of the MMC fundamental frequency, in order to achieve unity gain at low frequencies and reject high-frequency components. A phase lead filter $z^kS(z)$ is elaborately designed such that the natural frequency of the second order low pass filter $S(z)$ is f_n = 800 Hz and the time advance step is k = 8. The purpose of this phase lead filter is to improve the stability of the overall repetitive control system by achieving the desired frequency response shown in Fig. 8. $S(z)$ is used to shape the magnitude characteristics of the plant $P(z)$ so that the gain of $z^kS(z)P(z)$ is 0 dB at low frequencies and monotonically decreases at higher frequencies. The time advance unit z^k is used to compensate the phase delay caused by $S(z)$, the plant and the control system for larger overall system phase margin [23].

The system dynamic response and stability will be mainly determined by the repetitive gain K_r, which should be carefully designed [22]. In order to ensure the system stability at all frequencies, K_r has to be yielded [23] as

$$0<K_r\le\frac{1+\left|Q(e^{j\omega T_s})\right|}{\left|S(e^{j\omega T_s})P(e^{j\omega T_s})\right|} \tag{28}$$

Referring to the parameters in Table I, the theoretical range of K_r calculated based on (28) is zero to two, in which the overall control system can be stabilized. Equation (12) suggests that the convergence rate of the repetitive controller is inversely proportional to the magnitude of $Q(z)$-$K_rz^kS(z)P(z)$. It is obvious in Fig. 9 (a) that the convergence rate of the repetitive controller at frequencies lower than 1 kHz is highly affected by K_r. A K_r close to one provides relatively fast convergence for harmonics suppression at desired frequencies. The Bode diagram of the open loop transfer function of the differential current control is depicted in Fig. 9 (b). The phase margins of the differential current control loop with different values of K_r are indicated in the phase characteristics diagram. According to Fig. 9, K_r = 0.8 is selected with the consideration of both convergence rate and system stability (44° phase margin). The Nyquist plot of z^{Ns}-$Q(z)$+$K_rz^kS(z)P(z)$ in Fig. 10 indicates that the proposed repetitive control scheme is stable based on the parameters given in this subsection because the stability condition in (13) is always satisfied.

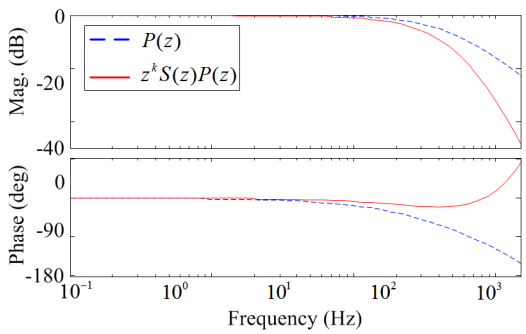

Fig. 8. Frequency characteristics of $P(z)$ and $z^kS(z)P(z)$.

IV. Simulation Results for Steady-State and Dynamic Performance

Simulation was conducted with Piecewise Linear Electrical

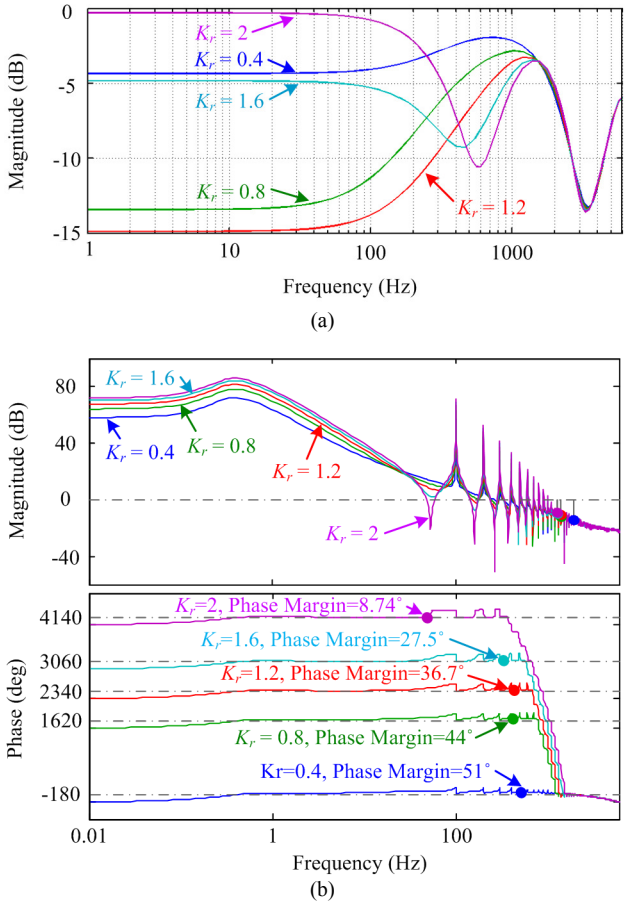

Fig. 9. Repetitive control system characteristics with different K_r: (a) Magnitude of $Q(z)$-$K_rz^kS(z)P(z)$; (b) Bode diagram of $[1+G_{rc}(z)]PI(z)G(z)$.

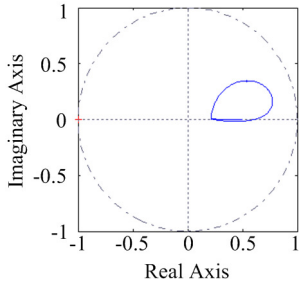

Fig. 10. Nyquist plot of z^{Ns}-$Q(z)$+$K_rz^kS(z)P(z)$.

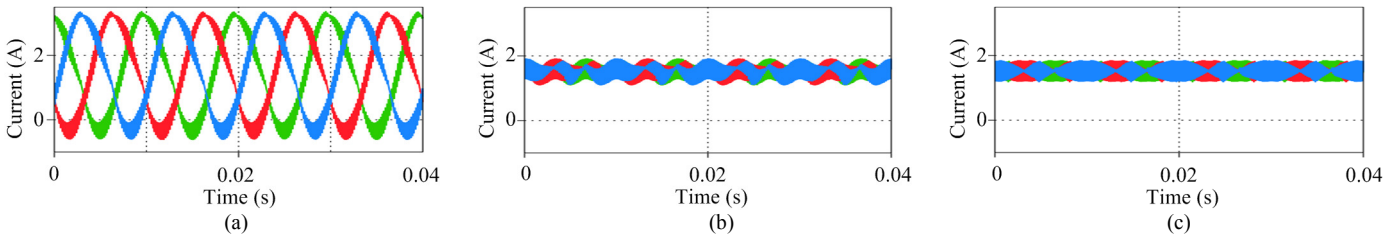

Fig. 11. Inner differential currents regulated by different controllers in simulation: (a) PI; (b) PI + 2nd R + 4th R; (c) Even-harmonic RC.

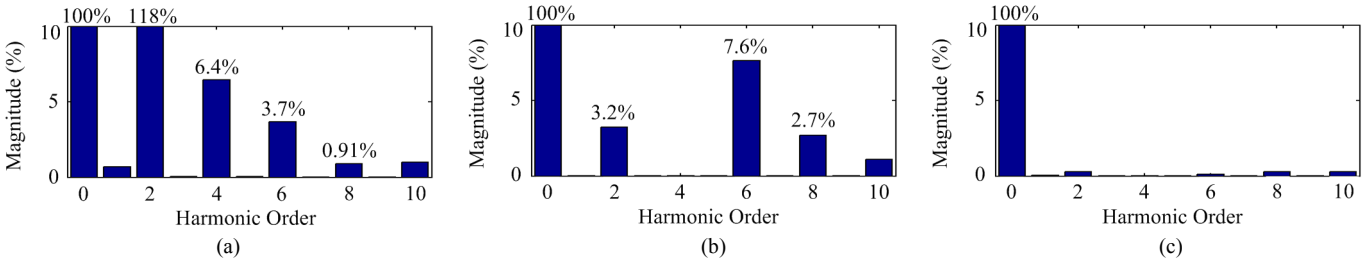

Fig. 12. Spectra of inner differential currents in phase *a* regulated by different controllers in simulation: (a) PI; (b) PI + 2nd R + 4th R; (c) Even-harmonic RC.

Circuit Simulation (PLECS) based on the MMC shown in Fig. 1 and system parameters listed in Table I. The main objectives were to show the effectiveness of the proposed repetitive control scheme in even-harmonic suppression, and its improved dynamic performance and tolerance to system frequency variation compared with the conventional repetitive controllers. All the simulation parameters and load conditions are the same as listed in Table I, except for a set of simulations under reference and load step changes.

Fig. 11 shows the inner differential currents in the phase leg regulated by different controllers, i.e. a PI controller, a PI controller with paralleled 2nd and 4th resonant controllers, and the even-order repetitive controller. The modulation index is set to be 0.833 to generate the output voltage with its peak value of 100 V. The harmonic spectra of the differential current in phase *a* are shown in Fig. 12. Fig. 12 (a) indicates that there are considerable even order harmonics in the differential current if only a PI controller is adopted, and there is basically negligible harmonics with frequencies higher than 500 Hz, which means that the cutoff frequencies of $Q(z)$ and $S(z)$ are properly designed to cope with current harmonics. The differential current can be less distorted by adding resonant controllers to suppress low order harmonics as shown in Fig. 11 (b). However, the higher order harmonics, e.g. 6th and 8th harmonics, may be even increased as shown in Fig. 12 (b). In contrast, the repetitive controller can almost completely eliminate the even harmonics in the circulating current, as shown in Fig. 11 (c) and Fig. 12 (c).

The startup process of the proposed and conventional repetitive controllers, when they are enabled at 0s, are illustrated in Fig. 13. The delay periods of the two controllers are half and one fundamental period respectively. t1 and t2 are the instants at which the repetitive controllers are actually activated and the controllers start to adjust their outputs

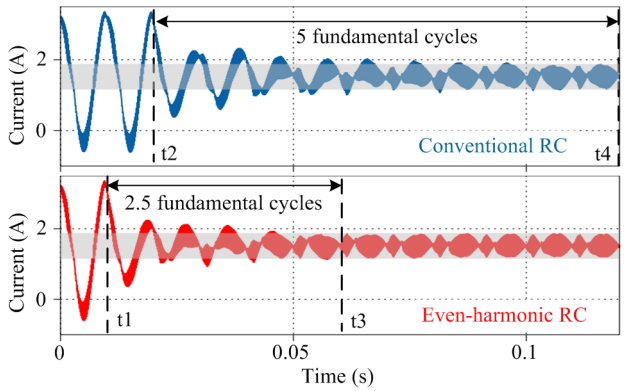

Fig. 13. Differential currents in phase *a* when the conventional and even-harmonic repetitive controllers are activated.

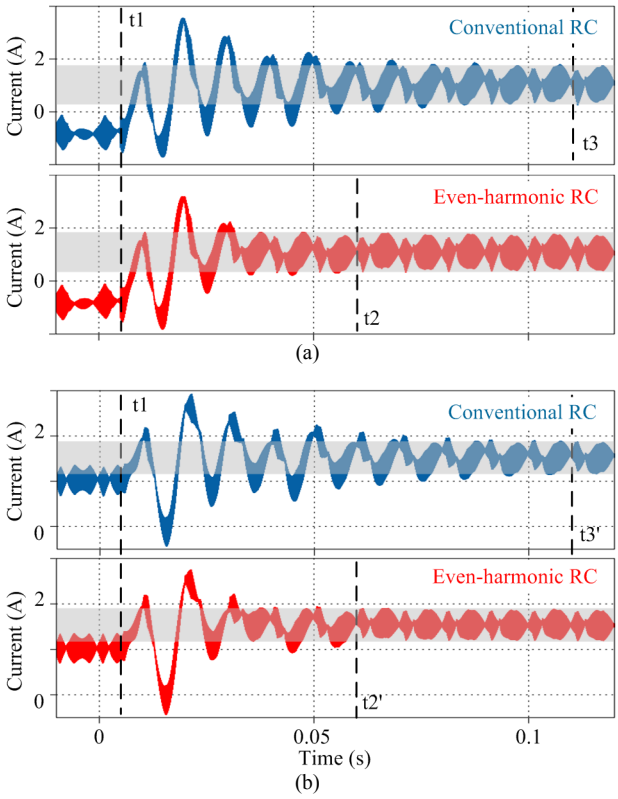

Fig. 14. Differential currents in phase *a* regulated by conventional and even-harmonic repetitive controllers during: (a) Modulation index step change: 0.5 – 0.833; (b) Load resistor step change: 20 Ω – 10 Ω.

according to tracking errors. It is obvious that the proposed repetitive controller only requires a half period (2.5 fundamental cycles) to achieve steady state after being activated as compared to that (5 fundamental cycles) of the conventional ones.

The inner differential currents regulated by the conventional and even-harmonic repetitive controllers under reference and load step changes are presented in Fig. 14. Fig. 14 (a) illustrates the current waveforms when the modulation index steps from 0.5 to 0.833. The current waveforms when the load resistance steps from 20 Ω to 10 Ω are shown in Fig. 14 (b). It can be seen in Fig. 14 that i_{diff} regulated by the even-harmonic repetitive controller is settled down at t2 and t2' while i_{diff} is settled down at t3 and t3' when a conventional repetitive controller is used. The proposed controller is stable during reference and load step changes. The halved N_s not only reduces the delay period of the repetitive controller but also speeds up the dynamic response of the system.

The performances of the both repetitive controllers under the condition of 5% frequency variation in the MMC output are shown in Fig. 15 (a). Fig. 15 (b) presents the fast Fourier transform (FFT) of the differential currents in phase *a*. The magnitude of the second order harmonic current, normalized to the DC component of the differential current, is reduced from 75.5% to 46.2% by replacing the conventional repetitive controller with the proposed one.

V. Experimental Results

The prototype of the single phase MMC as shown in Fig. 16 (a) was built in the laboratory. The experimental setup of the single phase MMC platform is shown in Fig. 16 (b). A dSPACE module DS1006 is adopted to implement the digital control and a DSP TMS320F28335 is used to generate the phase-shifted PWM signals for individual sub-modules. The parameters of the MMC system are listed in Table I. The equivalent arm resistors representing the losses in arms are not connected in the circuit. The modulation index of the output voltage was set to be 0.833 except for a set of experiments under reference and

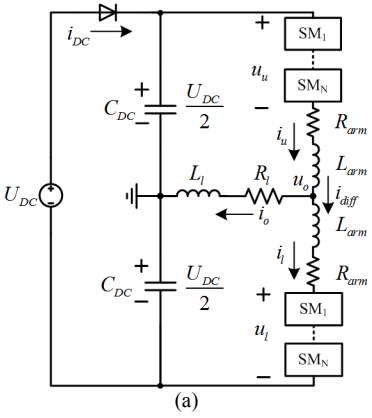

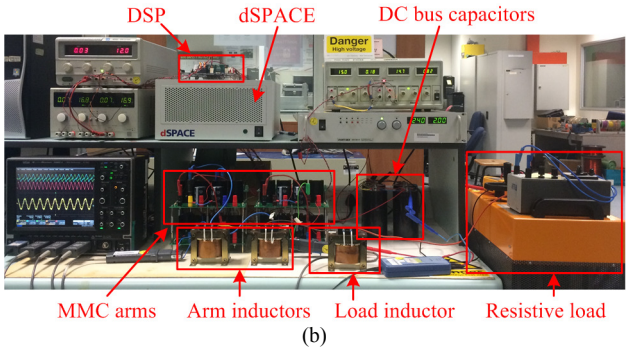

Fig. 16. Single phase MMC: (a) Schematics; (b) Experimental setup.

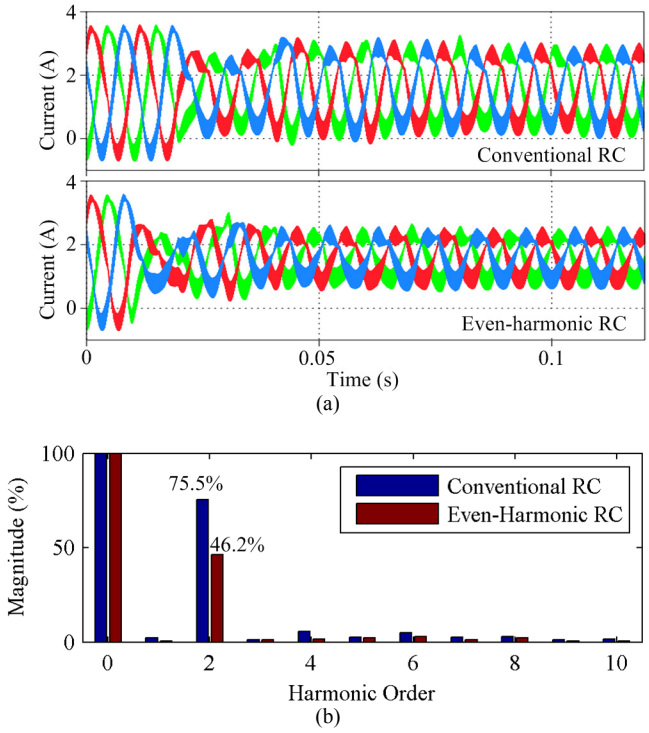

Fig. 15. Differential currents regulated by the conventional and even-harmonic repetitive controllers @ f_o = 47.5 Hz in simulation: (a) Differential currents; (b) Spectra of the differential currents in phase *a*.

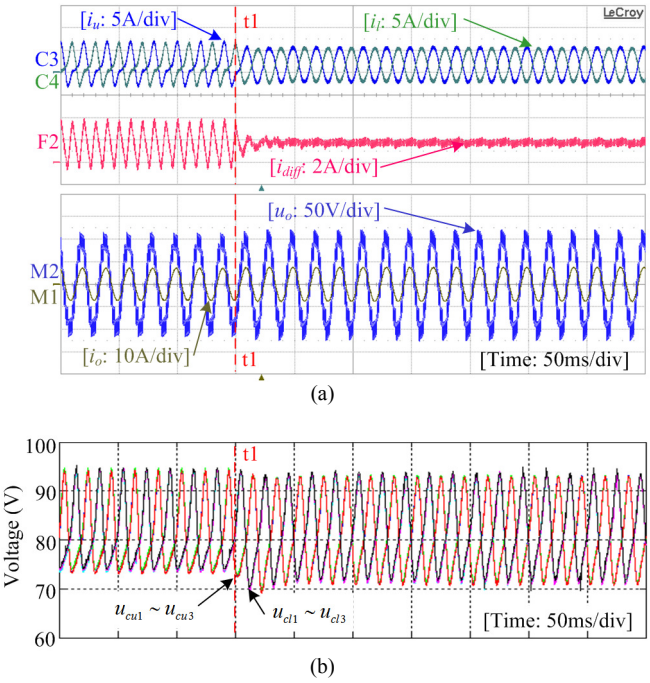

Fig. 17. Voltage and current waveforms of the MMC when the even-harmonic repetitive controller is activated at t1: (a) Arm currents, differential current, output voltage and current; (b) Sub-module capacitor voltages.

load step changes.

A. Steady-State Performance

Fig. 17 (a) presents the voltage and current waveforms of the MMC with the proposed even-harmonic repetitive control scheme activated at t1. It is obvious that the AC components of the differential current are reduced from 4.4 A to less than 0.8 A. The low-frequency harmonics in the circulating current are almost completely removed in a few fundamental cycles after t1. The high-frequency harmonics after t1 are mainly introduced by the switching of the semiconductor devices. The distortions in the arm currents are also removed, and only the DC and fundamental frequency components are retained as can be seen in Fig. 17 (a). The output voltage and current have been scarcely affected by the differential current even-harmonic repetitive control scheme. The sub-module capacitor voltages are sampled by the dSPACE because of the limitation of the channels of the oscilloscope.

The arm currents and inner differential current regulated by different controllers are presented in Fig. 18 and the spectra of corresponding differential currents are illustrated in Fig. 19. It can be seen in Fig. 19 (a) that even order harmonics (dominated by 2nd and 4th harmonics) exist in the differential current if only a conventional PI controller is adopted to regulate the differential current. The differential current controlled by a PI controller with paralleled 2nd and 4th resonant controllers is shown in Fig. 18 (b), where small low-frequency ripples can still be observed in i_{diff}. The spectrum in Fig. 19 (b) shows that the 2nd and 4th harmonics are well suppressed while more 6th harmonics can be found. The steady state performances of both conventional and even-harmonic repetitive controllers are almost the same and obviously better than that of PI and PR controllers, as shown in Fig. 18 (c) and (d). The harmonic spectra of these two repetitive controllers presented in Fig. 19 (c) and (d) are similar as well.

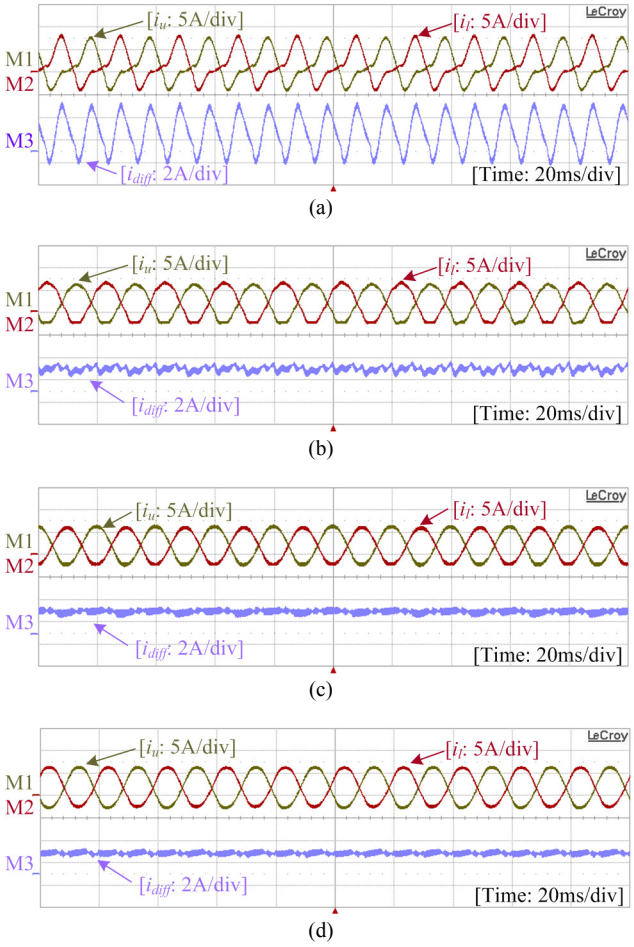

Fig. 18. Steady state arm currents and inner differential current regulated by different controllers: (a) PI; (b) PI + 2nd R + 4th R; (c) Conventional RC; (d) Even-harmonic RC.

B. Dynamic Response

The dynamic response of the repetitive control system is investigated in this set of experiments. The transients of the differential current while activating the conventional and even-harmonic repetitive controllers are illustrated in Fig. 20. After activating the repetitive controller at t = t1, the differential current regulated by the even-harmonic repetitive controller converges into the shadowed range smoothly by t = t2 (55 ms), while the harmonic contents are removed by the conventional

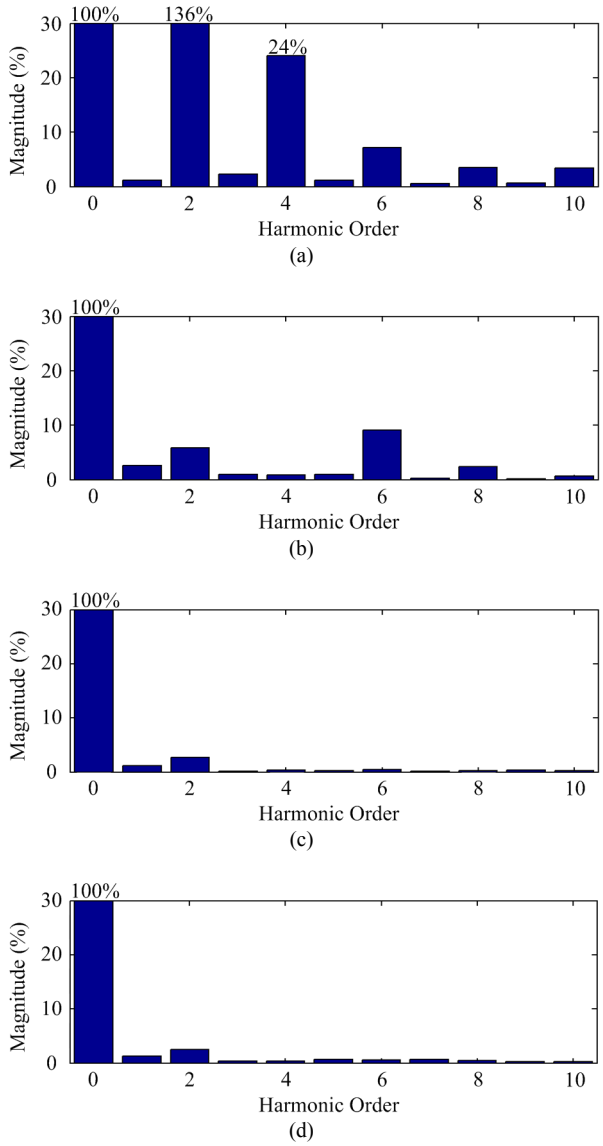

Fig. 19. Spectra of inner differential currents regulated by different controllers: (a) PI; (b) PI + 2nd R + 4th R; (c) Conventional RC; (d) Even-harmonic RC.

controller by t = t3 (115 ms).

The load inductance has been increased to be 16.3 mH in the following set of experiments in order to clearly show the dynamics of the control scheme under reference and load step changes with resistive-inductive loads. Fig. 21 presents the voltage and current waveforms of the MMC regulated by the two repetitive controllers when the output voltage reference steps from 0.5 to 0.833 at t1. The dynamic performances of the two controllers when the resistive load steps from 24 Ω to 12 Ω at t1 are shown in Fig. 22, where the power factor steps from 0.978 to 0.9198 as well. The overall control system is stable during reference and load step changes. It can be seen in both Fig. 21 and Fig. 22 that i_{diff} is settled down at t2 if it is controlled by an even-harmonic repetitive controller. On the other hand, i_{diff} is stabilized at t3 if a conventional repetitive controller is adopted. The results of this set of experiments show that the dynamic response of the proposed repetitive control system can be improved without severe transients.

C. *Performance under Frequency Deviation*

In Fig. 23, a frequency deviation of f_d = -2.5 Hz (-5%) is intentionally applied to the MMC output voltage reference while the repetitive controller is still designed for f_s = 50 Hz. The experimental results suggest that the even-harmonic repetitive controller has better performance in harmonic suppression, reflecting a greater tolerance for system frequency variation than that of the conventional one. As presented in Fig. 23 (b), the normalized second-order harmonic current can be reduced by 31.53% if the conventional repetitive controller is replaced by the proposed one when f_o = 47.5 Hz.

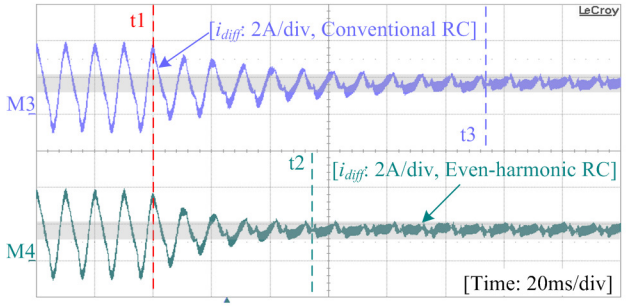

Fig. 20. Inner differential currents of the MMC when the conventional repetitive controller and even-harmonic repetitive controller are activated.

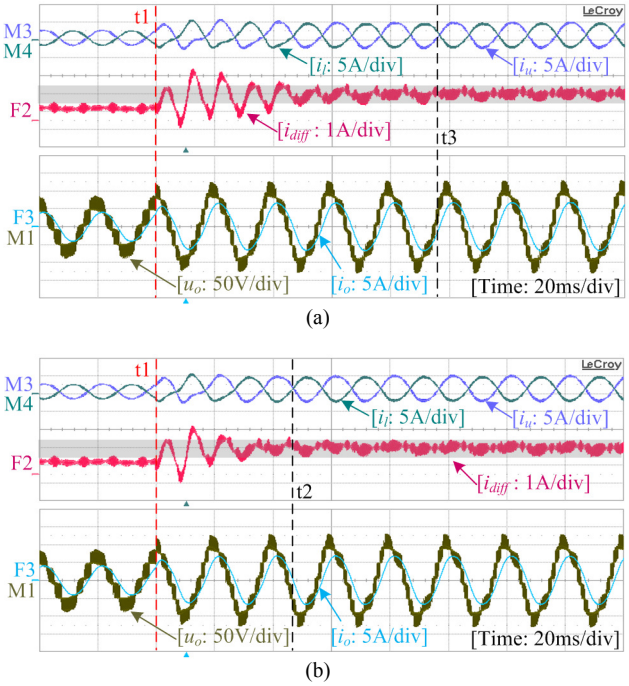

Fig. 21. Arm currents, differential current, output voltage and current waveforms during reference step change with: (a) Conventional repetitive controller; (b) Even-harmonic repetitive controller.

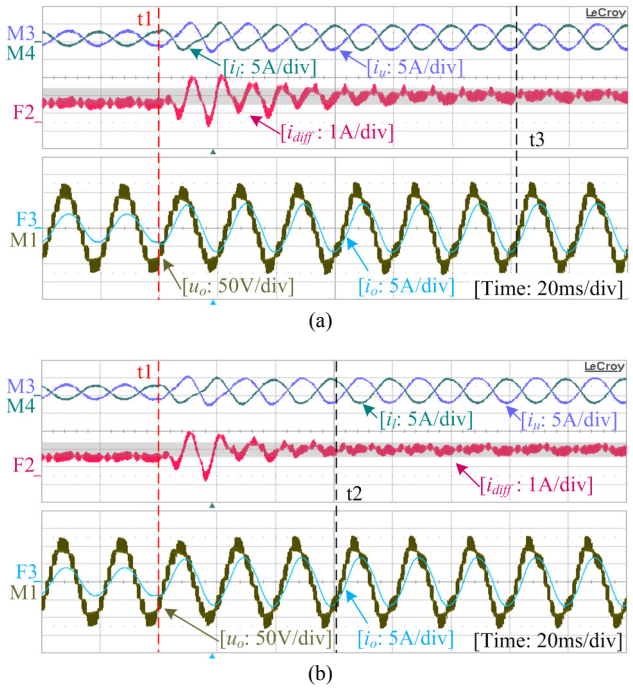

Fig. 22. Arm currents, differential current, output voltage and current waveforms during load step change with: (a) Conventional repetitive controller; (b) Even-harmonic repetitive controller.

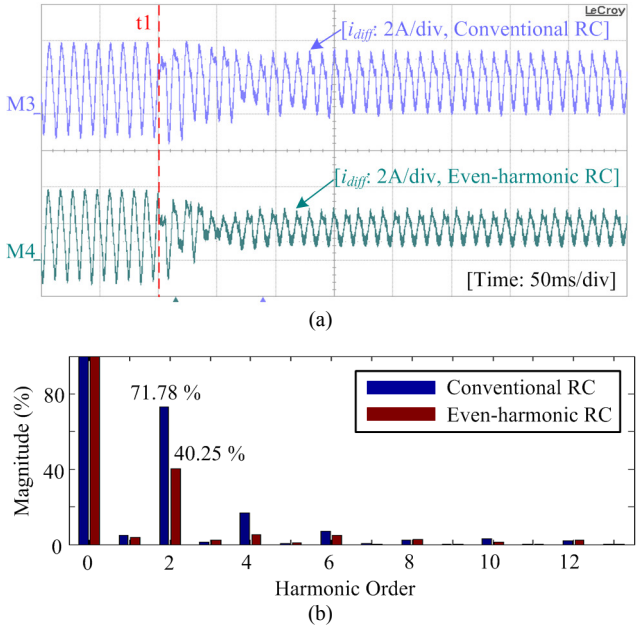

Fig. 23. Inner differential currents regulated by different repetitive controllers @ f_o = 47.5 Hz: (a) Waveforms of differential currents; (b) Spectra of differential currents.

VI. Conclusion

This paper has presented an even-harmonic repetitive control scheme that incorporates half delayed control cycle to suppress the even-order harmonics in the differential current of an MMC. The proposed control scheme not only removes the harmonics but also exhibits faster dynamic response and better performance under system frequency variation in comparison to those of conventional repetitive controllers. The analysis suggests that, by reducing the number of error sampling periods, the repetitive controller is improved in terms of less chip memory occupation, shorter controller delay period, faster convergence rate, higher low-frequency gain, higher crossover frequency, and wider control bandwidth at desired frequencies. The mathematical analysis, PLECS simulations, and experimental results agree with each other very well. The results show that the harmonics in the differential current are well suppressed, the dynamic response of the differential current control scheme is doubled, and the harmonic suppression performance under frequency variation is improved by more than 30% as compared to that of the conventional repetitive controllers.

References

[1] S. Kouro, M. Malinowski, K. Gopakumar, J. Pou, L. G. Franquelo, W. Bin, J. Rodriguez, M. A. Perez, and J. I. Leon, "Recent Advances and Industrial Applications of Multilevel Converters," *IEEE Trans. Ind. Electron.,* vol. 57, no. 8, pp. 2553-2580, Aug. 2010.

[2] G. Bergna, E. Berne, P. Egrot, P. Lefranc, A. Arzande, J. C. Vannier, and M. Molinas, "An Energy-Based Controller for HVDC Modular Multilevel Converter in Decoupled Double Synchronous Reference Frame for Voltage Oscillation Reduction," *IEEE Trans. Ind. Electron.,* vol. 60, no. 6, pp. 2360-2371, Jun. 2013.

[3] H. Saad, J. Peralta, S. Dennetiere, J. Mahseredjian, J. Jatskevich, J. A. Martinez, A. Davoudi, M. Saeedifard, V. Sood, X. Wang, J. Cano, and A. Mehrizi-Sani, "Dynamic Averaged and Simplified Models for MMC-Based HVDC Transmission Systems," *IEEE Trans. Power Del.,* vol. 28, no. 3, pp. 1723-1730, Jul. 2013.

[4] M. Hagiwara, K. Nishimura, and H. Akagi, "A Medium-Voltage Motor Drive With a Modular Multilevel PWM Inverter," *IEEE Trans. Power Electron.,* vol. 25, no. 7, pp. 1786-1799, Jul. 2010.

[5] H. P. Mohammadi, and M. T. Bina, "A Transformerless Medium-Voltage STATCOM Topology Based on Extended Modular Multilevel Converters," *IEEE Trans. Power Electron.,* vol. 26, no. 5, pp. 1534-1545, May. 2011.

[6] L. Harnefors, A. Antonopoulos, S. Norrga, L. Angquist, and H. P. Nee, "Dynamic Analysis of Modular Multilevel Converters," *IEEE Trans. Ind. Electron.,* vol. 60, no. 7, pp. 2526-2537, Jul. 2013.

[7] K. Ilves, A. Antonopoulos, S. Norrga, and H. P. Nee, "Steady-State Analysis of Interaction Between Harmonic Components of Arm and Line Quantities of Modular Multilevel Converters," *IEEE Trans. Power Electron.,* vol. 27, no. 1, pp. 57 - 68, Jan. 2012.

[8] Q. Tu, Z. Xu, and L. Xu, "Reduced Switching-Frequency Modulation and Circulating Current Suppression for Modular Multilevel Converters," *IEEE Trans. Power Del.,* vol. 26, no. 3, pp. 2009-2017, Jul. 2011.

[9] C. Wang, Q. R. Hao, and B. T. Ooi, "Reduction of low-frequency harmonics in modular multilevel converters (MMCs) by harmonic function analysis," *IET Generation Transmission & Distribution,* vol. 8, no. 2, pp. 328-338, Feb. 2014.

[10] Q. Song, W. H. Liu, X. Q. Li, H. Rao, S. K. Xu, and L. C. Li, "A Steady-State Analysis Method for a Modular Multilevel Converter," *IEEE Trans. Power Electron.,* vol. 28, no. 8, pp. 3702-3713, Aug. 2013.

[11] M. Hagiwara, and H. Akagi, "Control and Experiment of Pulsewidth-Modulated Modular Multilevel Converters," *IEEE Trans. Power Electron.,* vol. 24, no. 7, pp. 1737-1746, Jul. 2009.

[12] J. Pou, S. Ceballos, G. Konstantinou, V. G. Agelidis, R. Picas, and J. Zaragoza, "Circulating Current Injection Methods Based on Instantaneous Information for the Modular Multilevel Converter," *IEEE Trans. Ind. Electron.,* vol. 62, no. 2, pp. 777-788, Feb. 2015.

[13] K. Ilves, A. Antonopoulos, L. Harnefors, S. Norrga, L. Angquist, and H. P. Nee, "Capacitor voltage ripple shaping in modular multilevel converters allowing for operating region extension," in *IECON 2011 - 37th Annual Conference on IEEE Industrial Electronics Society*, 2011, pp. 4403-4408.

[14] J. Kolb, F. Kammerer, M. Gommeringer, and M. Braun, "Cascaded Control System of the Modular Multilevel Converter for Feeding Variable-Speed Drives," *IEEE Trans. Power Electron.,* vol. 30, no. 1, pp. 349 - 357, Jan. 2014.

[15] A. Antonopoulos, L. Angquist, L. Harnefors, and H. Nee, "Optimal Selection of the Average Capacitor Voltage for Variable-Speed Drives With Modular Multilevel Converters," *IEEE Trans. Power Electron.,* vol. 30, no. 1, pp. 227 - 234, Jan. 2014.

[16] B. Chen, Y. Chen, C. Tian, J. Yuan, and X. Yao, "Analysis and Suppression of Circulating Harmonic Currents in a Modular Multilevel Converter Considering the Impact of Dead Time," *IEEE Trans. Power Electron.,* vol. 30, no. 7, pp. 3542-3552, Jul. 2015.

[17] L. Angquist, A. Antonopoulos, D. Siemaszko, K. Ilves, M. Vasiladiotis, and H. P. Nee, "Open-Loop Control of Modular Multilevel Converters Using Estimation of Stored Energy," *IEEE Trans. Ind. Appl.,* vol. 47, no. 6, pp. 2516-2524, Nov./Dec. 2011.

[18] B. Bahrani, S. Debnath, and M. Saeedifard, "Circulating Current Suppression of the Modular Multilevel Converter in a Double-Frequency Rotating Reference Frame," *IEEE Trans. Power Electron.,* vol. 31, no. 1, pp. 783-792, Jan. 2016.

[19] R. Lizana, M. A. Perez, D. Arancibia, J. R. Espinoza, and J. Rodriguez, "Decoupled Current Model and Control of Modular Multilevel Converters," *IEEE Trans. Ind. Electron.,* vol. 62, no. 9, pp. 5382-5392, Sep. 2015.

[20] S. Li, X. Wang, Z. Yao, T. Li, and Z. Peng, "Circulating Current Suppressing Strategy for MMC-HVDC Based on Nonideal Proportional Resonant Controllers Under Unbalanced Grid Conditions," *IEEE Trans. Power Electron.,* vol. 30, no. 1, pp. 387-397, Jan. 2015.

[21] Z. Li, P. Wang, Z. Chu, H. Zhu, Y. Luo, and Y. Li, "An Inner Current Suppressing Method for Modular Multilevel Converters," *IEEE Trans. Power Electron.,* vol. 28, no. 11, pp. 4873-4879, Nov. 2013.

[22] K. Zhang, Y. Kang, J. Xiong, and J. Chen, "Direct repetitive control of SPWM inverter for UPS purpose," *IEEE Trans. Power Electron.,* vol. 18, no. 3, pp. 784-792, May. 2003.

[23] S. Yang, P. Wang, Y. Tang, and L. Zhang, "Explicit Phase Lead Filter Design in Repetitive Control for Voltage Harmonic Mitigation of VSI-based Islanded Microgrids," *IEEE Trans. Ind. Electron.,* vol. 64, no. 1, pp. 817-826, Jan. 2017.

[24] L. L. He, K. K. Zhang, J. J. Xiong, and S. S. Fan, "A Repetitive Control Scheme for Harmonic Suppression of Circulating Current in Modular Multilevel Converters," *IEEE Trans. Power Electron.,* vol. 30, no. 1, pp. 471-481, Jan. 2015.

[25] M. Zhang, L. Huang, W. Yao, and Z. Lu, "Circulating Harmonic Current Elimination of a CPS-PWM-Based Modular Multilevel Converter With a Plug-In Repetitive Controller," *IEEE Trans. Power Electron.,* vol. 29, no. 4, pp. 2083-2097, Apr. 2014.

[26] S. Yang, P. Wang, Y. Tang, M. Zagrodnik, X. Hu, and K. J. Tseng, "Even-harmonic repetitive control for circulating current suppression in Modular Multilevel Converters," in *2016 IEEE Applied Power Electronics Conference and Exposition (APEC)*, 2016, pp. 3591-3597.

[27] B. Li, D. Xu, and D. Xu, "Circulating current harmonics suppression for modular multilevel converters based on repetitive control," *Journal of Power Electronics,* vol. 14, no. 6, pp. 1100-1108, Nov. 2014.

[28] A. Lesnicar, and R. Marquardt, "An innovative modular multilevel converter topology suitable for a wide power range," in *Power Tech Conference Proceedings, 2003 IEEE Bologna*, 2003, p. 6 pp. Vol.3.

[29] D. Pan, X. Ruan, C. Bao, W. Li, and X. Wang, "Capacitor-Current-Feedback Active Damping With Reduced Computation Delay for Improving Robustness of LCL-Type Grid-Connected Inverter," *IEEE Trans. Power Electron.,* vol. 29, no. 7, pp. 3414-3427, Jul. 2014.

[30] S. Yang, P. Wang, and Y. Tang, "Feedback Linearization Based Current Control Strategy for Modular Multilevel Converters," *IEEE Trans. Power Electron.,* vol. PP, no. 99, pp. 1-1, Feb. 2017.

[31] K. Zhou, K. S. Low, D. Wang, F. Luo, B. Zhang, and Y. Wang, "Zero-phase odd-harmonic repetitive controller for a single-phase PWM inverter," *IEEE Trans. Power Electron.,* vol. 21, no. 1, pp. 193-201, Jan. 2006.

[32] B. Zhang, D. Wang, K. Zhou, and Y. Wang, "Linear Phase Lead Compensation Repetitive Control of a CVCF PWM Inverter," *IEEE Trans. Ind. Electron.,* vol. 55, no. 4, pp. 1595-1602, Apr. 2008.

[33] K. Zhou, and D. Wang, "Digital repetitive controlled three-phase PWM rectifier," *IEEE Trans. Power Electron.,* vol. 18, no. 1, pp. 309-316, Jan. 2003.

[34] G. F. Franklin, J. D. Powell, and A. Emami-Naeini, *Feedback Control of Dynamic Systems*, MA: Addison-Wesley, 1991.

[35] K. Ilves, L. Harnefors, S. Norrga, and H. Nee, "Analysis and Operation of Modular Multilevel Converters With Phase-Shifted Carrier PWM," *IEEE Trans. Power Electron.,* vol. 30, no. 1, pp. 268-283, Jan. 2015.

Shunfeng Yang (S'15) received the B.Eng. and M.Sc. degrees in Electrical Engineering from Southwest Jiaotong University, Chengdu, China, in 2007 and 2010, respectively. Since 2014, he has been with the School of Electrical and Electronic Engineering, Nanyang Technological University, Singapore, working towards the Ph.D. degree.
His research interests include power electronics, multi-level converters, and converter control techniques.

Peng Wang (M'00–SM'11) received the B.Sc. degree from Xi'an Jiaotong University, Xian, China, in 1978, the M.Sc. degree from the Taiyuan University of Technology, Taiyuan, China, in 1987, and the M.Sc. and Ph.D. degrees in power engineering from the University of Saskatchewan, Saskatoon, SK,Canada, in 1995 and 1998, respectively.
He is currently a Professor with the School of Electrical and Electronic Engineering, Nanyang Technological University, Singapore.

Yi Tang (S'10-M'14) received the B.Eng. degree in electrical engineering from Wuhan University, Wuhan, China, in 2007 and the M.Sc. and Ph.D. degrees from the School of Electrical and Electronic Engineering, Nanyang Technological University, Singapore, in 2008 and 2011, respectively.
From 2011 to 2013, he was a Senior Application Engineer with Infineon Technologies Asia Pacific, Singapore. From 2013 to 2015, he was a Postdoctoral Research Fellow with Aalborg University, Aalborg, Denmark. Since March 2015, he has been with Nanyang Technological University, Singapore as an Assistant Professor. He is the Cluster Director in advanced power electronics research program in the Energy Research Institute @ NTU (ERI@N).
Dr. Tang serves as an Associate Editor for the IEEE JOURNAL OF EMERGING AND SELECTED TOPICS IN POWER ELECTRONICS. He received the Infineon Top Inventor Award in 2012.

Michael Zagrodnik received the B.Eng. and M.Sc. degrees in electrical engineering from the University of British Columbia in 1984 and 1986, respectively.
He is currently a Project Manager at Rolls-Royce @ NTU Corporate Lab.
His main research interests include cooling system, multilevel converters, and marine propulsion.

Xiaolei Hu (S'10-M'15) was born in Wuhan, Hubei, People's Republic of China. He received B.E. and M.Sc from Electrical and Electronics Engineering school of Huazhong University of Science and Technology in 2006 and 2008 respectively. He was with Delta Power Electronics Center Shanghai from Jul. 2008- Aug. 2010 as an electrical engineer.
He was awarded Ph.D. degree in engineering by Nanyang Technological University, Singapore at 2015. He worked as a research staff in Rolls-Royce corporate lab at NTU from 2014 to 2015. He is current with Energy Research Institute @ Nanyang Technological University, Singapore.

Born in Singapore, **King-Jet** received B.Eng. (First Class) and M.Eng. from National University of Singapore, and Ph.D. from Cambridge University in England. He has more than 25 years of academic, research, industrial and professional experience in electrical power and energy systems. He has undertaken numerous contract research projects for major corporations such as Vestas, Rolls-Royce and Bosch, and has been holding key advisory appointments in both public and private sector in Singapore. He has been awarded numerous research grants and published over 250 technical papers, and actively reviews and edits papers for major international journals and conferences. He was appointed the Head of Power Engineering Division in Nanyang Technological University for the maximum term of six years. He has been the Board Member of the Singapore Green Building Council, of the Advisory Board of BCA Centre for Sustainable Buildings, and the Energy Standards Committee of Spring Singapore. He has been program co-leader of Singapore-Berkeley Building Efficiency and Sustainability for the Tropics (SinBerBEST) at Singapore's NRF-CREATE, and the founding Director of Electrical Power Systems Integration Laboratory @ NTU, a Rolls-Royce research facility. He has also founded a number of start-up companies.
Dr Tseng is Fellow of Institution of Engineering and Technology (FIET), Fellow of Institution of Engineers Singapore (FIES), and Fellow of Cambridge Philosophical Society, as well as a Chartered Engineer registered in UK. He has held a number of major appointments in professional societies including the Chair of IEEE Singapore Section in 2005. He was awarded the Swan Premium by the IET, the IEEE Third Millennium Medal, the IEEE Region Ten Outstanding Volunteer Award, and the Long Service Medal (Education) from the Singapore Government. Currently, he is also the Professor and Director of Electrical Power Engineering at Singapore Institute of Technology.